

Harnessing Multi-resolution and Multi-scale Attention for Underwater Image Restoration

Alik Pramanick, Arijit Sur and V. Vijaya Saradhi

Department of Computer Science and Engineering, Indian Institute of Technology Guwahati, India.

*Corresponding author(s). E-mail(s): p.alik@iitg.ac.in;
Contributing authors: arijit@iitg.ac.in; saradhi@iitg.ac.in;

Abstract

Underwater imagery is often compromised by factors such as color distortion and low contrast, posing challenges for high-level vision tasks. Recent underwater image restoration (UIR) methods either analyze the input image at full resolution, resulting in spatial richness but contextual weakness, or progressively from high to low resolution, yielding reliable semantic information but reduced spatial accuracy. Here, we propose a lightweight multi-stage network called Lit-Net that focuses on multi-resolution and multi-scale image analysis for restoring underwater images while retaining original resolution during the first stage, refining features in the second, and focusing on reconstruction in the final stage. Our novel encoder block utilizes parallel 1×1 convolution layers to capture local information and speed up operations. Further, we incorporate a modified weighted color channel-specific l_1 loss (cl_1) function to recover color and detail information. Extensive experimentations on publicly available datasets suggest our model's superiority over recent state-of-the-art methods, with significant improvement in qualitative and quantitative measures, such as **29.477** dB PSNR (**1.92%** improvement) and **0.851** SSIM (**2.87%** improvement) on the EUVP dataset. The contributions of Lit-Net offer a more robust approach to underwater image enhancement and super-resolution, which is of considerable importance for underwater autonomous vehicles and surveillance. The code is available at: <https://github.com/Alik033/Lit-Net>.

Keywords: Underwater image enhancement, super-resolution, multi-scale, multi-resolution, channel-specific loss

1 Introduction

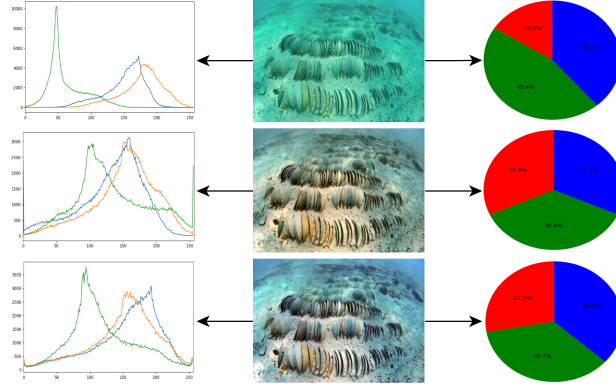


Fig. 1 First row represents the tricolor histogram and pie chart of the degraded underwater image, second row represents the tricolor histogram and pie chart of the enhanced underwater image by our Lit-Net, and third row represent the tricolor histogram and pie chart of the ground-truth image.

In the recent past, underwater vision has become an emerging research topic. Autonomous underwater vehicles (AUVs) need to understand their operating environment in various applications, such as monitoring marine life and reefs, examining submarine cables and wreckage, and collaborating with humans. The above-mentioned applications are performed by executing high-level vision tasks on underwater images and videos, such as object classification [1], detection [2], segmentation [3], etc. Visual degradation may have an adverse effect on these high-level vision tasks.

Even though advanced cameras are commonly used in underwater photography and videography, improved clarity is still needed due to the limited visibility caused by light bending, absorption, and scattering, which can cause distortions in the captured images and videos. One of the primary reasons for the visual distortions in underwater imaging is the non-uniform attenuation of light, which varies depending on the wavelength of the light [4]. Further, in the underwater scenario, blue color traverses longer than other colors as its wavelength is the shortest. The prevalence of blue and green colors in underwater imagery directly impacts the effectiveness of higher-level tasks [5]. Fig. 1 demonstrates the tricolor histogram and pie chart color distribution of a degraded underwater image, an enhanced version of the same image, and the ground truth image, respectively. There is a noticeable issue with color casting in underwater images. As a result, underwater images are often of low contrast, blurry, bluish, greenish, etc. In order to tackle these issues, it is necessary to employ efficient low-level computer vision techniques such as image enhancement, super-resolution, and other similar methods.

In recent research, deep learning-based methods have exhibited remarkable outcomes when applied to low level vision tasks. It has been noticed that a lot of State-of-the-art Underwater Image Restoration (UIR) works process the R-G-B channels with the same receptive field sizes. However, the same receptive fields for each

R-G-B channel may not be suitable in most underwater situations. Sharma et al. [6] have shown that different sizes of receptive fields help in UIR. Still, it needs to capture the desired global effects that require considering the relationships between color components. Deep neural networks designed for UIR are broadly categorized into the single scale (high-resolution) [6–8] or an encoder-decoder feature processing [9–11]. High-resolution (single-scale) networks avoid down-sampling, resulting in images with more spatially precise information. However, these networks become less beneficial at encoding semantic information. For encoder-decoder based approaches, the encoder gradually maps the input to a low-resolution representation, and the decoder reverses the mapping to obtain the original resolution. These strategies grasp a broad context by reducing spatial resolution; however, finer spatial details are lost, making image reconstruction harder.

Underwater image restoration is a technique that requires pixel-to-pixel correspondence between the input and output images and is sensitive to the position of pixels. Knowing that the underwater images are mainly bluish and greenish, removing only the undesired degraded content is crucial while preserving all the essential spatial information, including true edges and texture. For this, different sizes of receptive fields are used for different color channels (such as R (3×3), G (5×5), and B (7×7)) in the proposed architecture. This helps us achieve multi-resolution analysis for different color channels to maintain spatial (high-resolution) information and capture the local and global context. Additionally, we process the whole RGB image with 1×1 convolution to capture the desired global effects considering the relationships between color components. However, a 1×1 convolution outputs an image with the same width and height as the input. It acts as a channel collapse as well as a color messenger to the preceding layers [12]. A new multi-scale strategy is incorporated to maintain semantic (encoder-decoder) information. Apart from that, we use the 1×1 convolution layer in our encoder network to speed up the number of operations. Furthermore, we have incorporated attention-based skip connections for more discriminative representations.

Fig. 2(a) visually compare the proposed scheme and recent best-published works on the low-contrast real underwater image. It is observed that the proposed Lit-Net method produced visually more accepted results than recent best-published works. Fig. 2(b) illustrates similar comparison results for the underwater image super-resolution (UISR) method. It is observed that most of the existing methods generate a greenish tone in their resulting image, while Lit-Net yields a visually improved color-corrected result. The major contributions of this work is outlined as follows:

- We propose a lightweight multi-stage network for underwater image enhancement and super-resolution. The first stage is used for multi-resolution image analysis while retaining its original resolution. The second stage enhances the intermediate features while retraining the important information. The last stage focus on the reconstruction of the enhanced and super-resolved image.
- We design a novel encoder block where each encoder layer has four parallel 1×1 convolution layers to pay attention to the dominant color and capture the local information precisely. It also speeds up the number of operations as it is less expensive than the larger-size of filters.

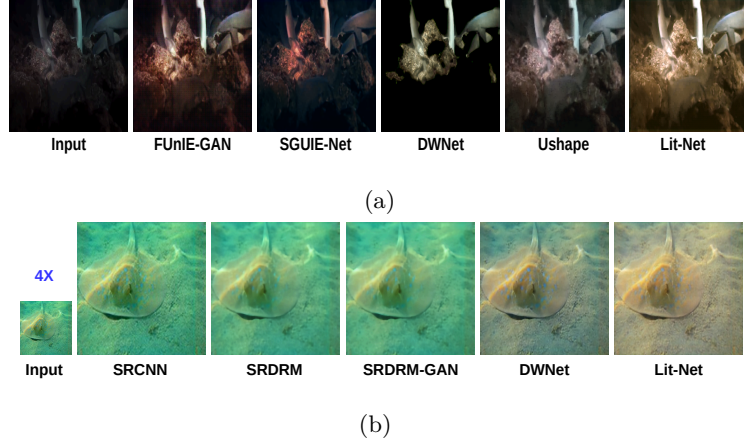


Fig. 2 Visual comparisons of (a) enhancement example on low contrast underwater image, (b) 4x super-resolve example on underwater image. The proposed Lit-Net model enhanced the contrast and removes the color deviation.

- We modified the l_1 loss function to a weighted color channel specific l_1 loss (cl_1) function. It helps to recover the color and detail information.

We provide extensive experiments against the best-published state-of-the-art in underwater image enhancement (UIE) and UISR to show the benefit. The performance of the proposed model has been demonstrated by comparing it with existing methods through various tasks, including underwater semantic segmentation and object detection.

2 Related Work

In this section, we briefly describe the overview of prior research on UIR. The two main parts of this literature are (1) underwater image enhancement and (2) underwater single-image super-resolution.

2.1 Underwater Image Enhancement

Earlier, approaches are separated as physical model-based or physical model-free types. Physical model-based techniques [13–17] typically use an imaging model and estimate the attenuation light and transmission map with hand-crafted priors to restore underwater images. The commonly used priors are the dark channel prior (DCP) [18–20] and its modified versions red channel prior [21], blurriness prior [17], light attenuation prior [22], transmission prior [23]. Derya et al. [24] aims to retrieve color with the revised model using RGBD images. However, statistical priors may perform poorly in difficult underwater situations, and the optical image formation model may yield errors due to irregular scene effects [25, 26].

Physical model-free strategies include multi-scale fusion that combines information from different levels of resolution [27–29], variational optimization that involves the optimization of a cost function with respect to a set of parameters [30], the work

proposed in pixel distribution adjustment [31, 32], focus on altering image intensity values to make them more realistic. The absence of the underwater imaging model in physical model-free techniques can create unwanted visual anomalies due to the interference of noise in the underwater environment.

In recent times, deep learning-based approaches for underwater image enhancement have achieved substantial gains [7, 9, 11, 33–41]. Previous studies have utilized Generative Adversarial Networks (GANs) to address the issue of inadequate underwater images and their corresponding clean image pairs. By using GANs, they synthesize underwater image datasets or execute unpaired training. In [42], they used GAN [43] to generate the large synthetic dataset and proposed a two-stage architecture for color correction of monocular underwater images. Liu et al. [44] used the Cycle-GAN [45] to produce roughly 4000 pairs of synthetic underwater degraded and ground truth images. Also, they proposed UResnet, which would use residual learning to improve underwater images. Their UResnet used the VDSR [46] model (presented for the super-resolution model). [37] presented a straightforward classifier to produce the GAN model better discriminative for various water types. The authors of [47] proposed a conditional GAN approach that relies on the attention [48, 49] mechanism for the activity of UIR. The work proposed in [50] suggested the use of a spiral Generative Adversarial Network based network for UIE. Li et al. [7] created the Underwater Image Enhancement Benchmark (UIEB) dataset, which is a comprehensive dataset of real-world underwater images for the purpose of UIE. Further, the work in [7] proposed Water-Net, a gate fusion CNN-based model for UIE by fusing three enhanced inputs: (a) gamma-corrected input, which affects the overall brightness and contrast of the image, (b) white-balanced input, which ensure that the colors in an image appear accurate and natural, regardless of the lighting conditions under which the image was taken, and (c) histogram equalized input. Islam et al. [11] presented the EUVP dataset containing 20K underwater images. Also, [11] introduced a conditional GAN-based fully-convolutional framework for UIE in real time. To address color cast and low contrast degradation concerns [34] proposed a multi-color space encoder framework that incorporates an attention mechanism to merge the attributes of various color spaces into a cohesive structure and adaptively choose the most significant features. Recently, Huo et al. [51] presented a deep learning model that progressively refines underwater images using a wavelet boost learning technique in spatial and frequency domains. Qi et al. [52] proposed SGUIE-Net for UIE, in which they introduced semantic information as high-level guidance.

2.2 Underwater Image Super-resolution

The objective of Single Image Super-Resolution (SISR) is to improve the resolution of a low-quality image by generating a higher resolution version of the same image [53–56]. Li et al. [7] proposed SRCNN, the initial Super-Resolution (SR) model utilized a Color Features-based methodology and Multi-Layer Perceptron (MLP) technique. The work in [57] proposed an SR network based on wavelet transform that decomposes an image into a series of wavelets that vary in scale and frequency and improve dense block structure. Lu et al. [58] initially offered a self-similarity SR algorithm to the LR images for HR images. Finally, they got the SR images by applying a convex fusion rule that

combines multiple estimates or observations into a single estimate of the HR images. The authors of [59] build a multi-modal optimization technique for underwater super-resolution that quantifies the perceptual quality of the image based on factors such as global content, color, and local style information to create an adversarial training pipeline. Islam et al. [8] presented a generative framework based on residual-in-residual networks that simultaneously improve and super-resolving underwater imagery for better visual perception. Sharma et al. [6] presented a deep learning-based framework using CNN, which consists of multiple stages, and it employs the distinct size of the kernel to each R-G-B color channel of an image, guided by its wavelength for concurrent UIE and UISR task. Recently, Zang et al. [60] proposed a multi-path network guided by an attention module that mainly utilizes the cross-convolution technique for UISR.

2.3 Major Observation

Despite significant advancements in the enhancement of underwater images, current approaches still suffer from visual artifacts, such as color distortion, poor visibility, low contrast, and hazy. These are not particularly efficient in improving images that are severely degraded and lacking in texture. In such instances, the resulting images may be over-saturated due to the amplification of noise. While the correction of hue is typically accurate, there is still a deficiency in the restoration of both texture and color. Within a GAN-based model [11, 61], the discriminator can become overly proficient too quickly, leading to a decrease in the gradient effect and ultimately inhibiting the generator’s ability to learn. In such instances, the produced images often exhibit poor color uniformity and inadequate texture details. In [52], they use a segmentation mask with a degraded image to produce the enhanced result. Generating the segmentation mask itself will take time, and if we use a pre-trained segmentation module, it won’t produce good segmentation for a diverse set of underwater images, which will affect the UIE performance. In the case of UISR, even though efforts have been made to super-resolve the images, they often contain unwanted artifacts, such as a lack of representation of texture features and high-frequency information. Due to variations in attenuation ranges across channels, underwater images require special considerations that differ from those necessary for outdoor images. As a result, directly applying outdoor models [62–64] may not be appropriate in underwater settings. Inspired by [6], we have shown how the different receptive field sizes help to gain performance in both UIE and UISR. Also, we have shown how the lightweight encoder-decoder based model with attention-based skipped connection is sufficient to generate notable performance gain in both tasks. Taking into account structural appropriateness and texture similarity, the proposed approach can generate high-quality results without the need for any post-processing operations.

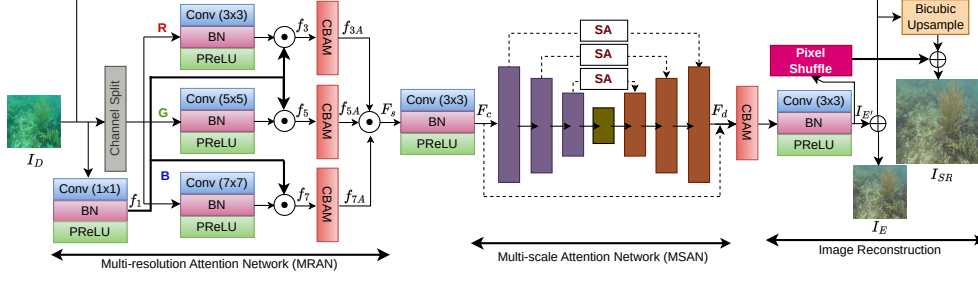


Fig. 3 Overview of our proposed model for UIE and UISR. The model accepts a degraded underwater image as input and produces an improved image that is visually and spatially enhanced.

3 Proposed Method

3.1 Network Architecture

In this work, a deep learning-based architecture is proposed to enhance and super-resolve underwater images. The overall architecture is depicted in Fig. 3. We divided the network into three distinct modules as follows:

- Multi-resolution Attention Network (MRAN)
- Multi-scale Attention Network (MSAN)
- Image Reconstruction

The Multi-resolution Attention Network (MRAN) extracts shallow features that correspond to low-frequency details from the input degraded underwater image (I_D). The purpose of MRAN is to analyze the input image in a multi-resolution way while maintaining its original resolution. To obtain the most prominent features, followed by the MRAN module, we design a multi-scale attention network (MSAN) by extracting the rich features related to high-frequency details from the input image while retraining the important information through attention-based skipped connection. Finally, an image reconstruction module is devised to restore the enhanced and super-resolved image.

3.1.1 Multi-resolution Attention Network

In the proposed multi-resolution attention network (MRAN), we directly use full-resolution input images to characterize multi-resolution feature representations using different kernel sizes (having different receptive fields) for analyzing the global and local information. This module incorporates four convolutional layers using four different kernel sizes of 1×1 , 3×3 , 5×5 , and 7×7 with batch normalization and PReLU activation. We generate the R, G, and B channel-specific features with 3×3 , 5×5 , and 7×7 kernels. Also, we extract the features from the whole RGB image with 1×1 kernel. Then, we concatenate RGB features with channel-specific features. The concatenated features are passed through attention blocks and finally concatenated to get the output of the MRAN block. Shallow contextual features (F_s) are acquired

given the input I_D .

$$F_s = f_{3A} \odot f_{5A} \odot f_{7A}, \quad (1)$$

where, \odot indicates the concatenation operation and the attentive contextual features (f_{kA}) with receptive field size k can be estimated as

$$\begin{aligned} f_{3A} &= A_n(f_3) \\ f_{5A} &= A_n(f_5) \\ f_{7A} &= A_n(f_7) \end{aligned} \quad (2)$$

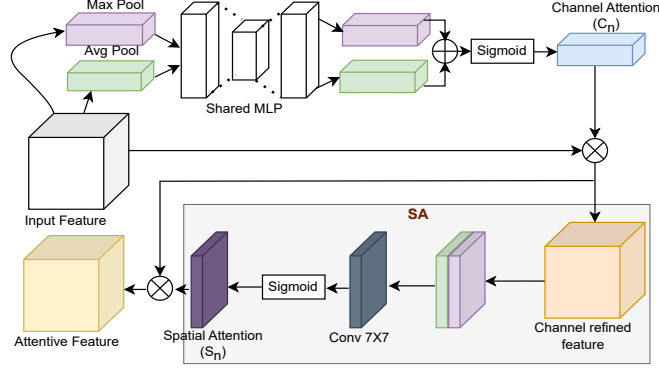


Fig. 4 Network architecture of CBAM block [65].

We use CBAM [65] module as an attention block (A_n) to refine the obtained features f_k . The architecture of CBAM is shown in Fig. 4. CBAM inputs an intermediate feature map to retrieve the channel and spatial attention features. The purpose of channel attention is to focus on identifying the important features present in an input image. It aims to determine 'what' aspects of the image are significant in terms of representing the desired information. Spatial attention concentrates on 'where' is an informative part. We recommend that readers refer to [65] for more information on CBAM. The refine features f_k can be computed as

$$\begin{aligned} f_1 &= p_r(b_n(c^{1 \times 1}(I_D))) \\ f_3 &= p_r(b_n(c^{3 \times 3}(I_D^R))) \odot f_1 \\ f_5 &= p_r(b_n(c^{5 \times 5}(I_D^G))) \odot f_1 \\ f_7 &= p_r(b_n(c^{7 \times 7}(I_D^B))) \odot f_1 \end{aligned} \quad (3)$$

where $c^{k \times k}$, b_n , and p_r represent a convolution operation, batch normalization [66] and parametric ReLU layers, respectively. $k \times k$ indicates the kernel size. I_D^C ($C \in R, G, B$) indicates the individual channel of a degraded image.

The output generated by MRAN is first fed into a convolution layer, which is then used as input for MSAN.

$$F_c = p_r(b_n(c^{3 \times 3}(F_s))) \quad (4)$$

3.1.2 Multi-scale Attention Network

The proposed MSAN module is a UNet-like architecture where each encoder and corresponding decoder layer is linked with an attention-based skipped connection. In this work, a novel extension (refer to Fig. 5) is used in each encoder layer to analyze the different input resolutions more accurately. To do this, we map the high-resolution feature (F_c) to a low-resolution representation and slowly retrieve the high-resolution representation from the lower level. Generally, the encoder-decoder process learns semantically-rich feature representation (f_{ds}) (multi-scale contextual information), but it is not spatially precise due to down-sampling. To get both semantically and spatially richer features (F_d), the features map f_{ds} is concatenated with the high-resolution features map (F_c). Also, to ensure the feature re-usability, we use spatial attention-based skip connection, as in Fig. 3. The output of MSAN can be estimated as

$$F_d = F_c \odot f_{ds} \quad (5)$$

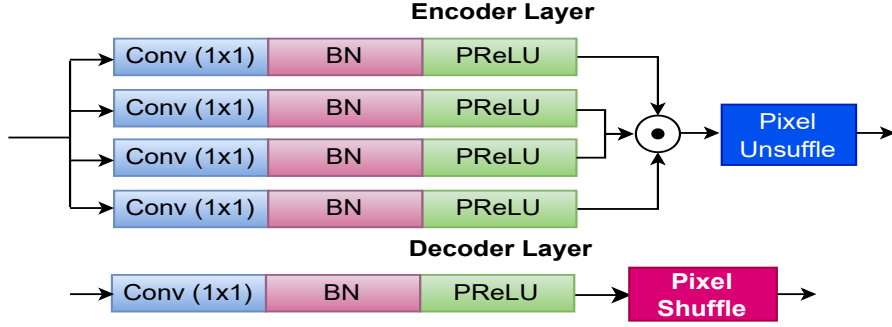


Fig. 5 Network architecture of proposed encoder and decoder layer.

We have modified each encoder layer (refer to Fig. 5). Generally, a normal encoder layer uses a 3×3 convolutional layer and a maxpool layer which is computationally costly because of 3×3 kernel. Here, each encoder layer contains four 1×1 convolution layers in parallel. Finally, we concatenated the four convoluted features and passed them through a pixel unshuffle layer. Instead of a maxpool layer, we use pixel-unshuffle to downsample each feature to minimize the information loss. We use three encoder

layers in our MSAN. Mathematically, the encoder is formulated as

$$\begin{aligned}
E_1^1 &= p_r(b_n(c^{1 \times 1}(F_c))) \\
E_1 &= P_{unshuffle}(E_1^1 \odot E_1^1 \odot E_1^1 \odot E_1^1) \\
E_2^1 &= p_r(b_n(c^{1 \times 1}(E_1))) \\
E_2 &= P_{unshuffle}(E_2^1 \odot E_2^1 \odot E_2^1 \odot E_2^1) \\
E_3^1 &= p_r(b_n(c^{1 \times 1}(E_2))) \\
E_3 &= P_{unshuffle}(E_3^1 \odot E_3^1 \odot E_3^1 \odot E_3^1)
\end{aligned} \tag{6}$$

where E_i^1 represents the each branch of each encoder layer E_i ($i = 1, 2, 3.$) and $P_{unshuffle}$ indicates the pixel-unshuffle operation. The output of the encoder can be computed as

$$B_{kn} = p_r(b_n(c^{1 \times 1}(E_3))) \tag{7}$$

Let S_n represent the spatial attention module and $P_{shuffle}$ represents the pixel shuffle operation as an up-sampling operation to increase the spatial resolution. The decoder can be defined as

$$\begin{aligned}
D_1 &= P_{shuffle}(B_{kn}) \odot S_n(E_3) \\
D_2 &= P_{shuffle}(D_1) \odot S_n(E_2) \\
f_{ds} = D_3 &= P_{shuffle}(D_2) \odot S_n(E_1)
\end{aligned} \tag{8}$$

where, D_i ($i = 1, 2, 3.$) indicates the each decoder layer.

3.1.3 Image Reconstruction

The final stage of the proposed model is used as the reconstruction module. In the case of underwater image enhancement, it takes the output features of MSAN (F_d) as input and feeds them into a convolutional layer to produce residual image ($I_{E'}$). Finally, the enhanced image is obtained by $I_E = (I_{E'}) + I_D$, where

$$I_{E'} = p_r(b_n(c^{3 \times 3}(F_d))) \tag{9}$$

We use three channels to get enhanced underwater images. In the case of underwater image super-resolution, we use $3s^2$ (s indicates the scale factor) channel for equation 9 as it upsampled the MSAN features to the desired resolution. After that, we use pixel-shuffle [67] layers to refine the spatial quality of the image further. The purpose of this layer is to enhance the resolution and details of the image. Also, we use bicubic up-sampling to improve the spatial resolution of the I_D . Finally, the super-resolved image (I_{SR}) is obtained by

$$I_{SR} = P_{shuffle}(I_E) + U_{bicubic}(I_D) \tag{10}$$

3.2 Loss Function

3.2.1 Weighted Color channel specific L1 loss

It is observed in the literature that the l_2 loss function can lead to the appearance of blurry artifacts in the resulting enhanced images. Due to this, we have chosen to employ l_1 loss rather than l_2 loss. To train Lit-Net, instead of using simple l_1 loss, we have used weighted color channel-wise l_1 loss for reconstructing high-quality underwater images. This is because underwater images can be affected differently by the water medium in each channel, and thus, the cl_1 loss enables the model to focus more on the channels that are dominated in underwater. The weighted channel-specific l_1 loss can be expressed as follows:

$$cl_1 = w_r l_{1_r} + w_g l_{1_g} + w_b l_{1_b} \quad (11)$$

where, l_{1_r} , l_{1_g} , and l_{1_b} indicates the red (r), green (g), and blue (b) channel specific l_1 loss, these can be formulated as

$$\begin{aligned} l_{1_r} &= \frac{1}{n} \sum_{i=1}^n \|ES(I_{D_i})_r - (I_{O_i})_r\|_1 \\ l_{1_g} &= \frac{1}{n} \sum_{i=1}^n \|ES(I_{D_i})_g - (I_{O_i})_g\|_1 \\ l_{1_b} &= \frac{1}{n} \sum_{i=1}^n \|ES(I_{D_i})_b - (I_{O_i})_b\|_1 \end{aligned} \quad (12)$$

where $ES(.)$ represents the process of Lit-Net, I_O is the original clean image in the case of UIE, and the higher-resolution image in the case of UISR. Empirically, we have set w_r , w_g , and w_b to be equal to 1, 1.5, and 2, respectively.

3.2.2 Perceptual loss

Although training with pixel loss enhances PSNR, it does not improve perceptual quality. To address this flaw, we integrated the Perceptual loss [68] to make it more perceptually improved. This loss function helps to ensure that the enhanced image maintains its fine details and textures. To accomplish this goal, we have used pre-trained VGG16 ($V_f(\phi)$) [69] model, which is pre-trained on a large-scale image database (ImageNet). We define the cost function as the Euclidean distance between the relu2.2 features obtained from the predicted image and the actual clean image, and it can be expressed as follows:

$$l_p = \frac{1}{n} \sum_{i=1}^n \|V_f(ES(I_{D_i}); \phi) - V_f(I_{O_i}; \phi)\|_2^2 \quad (13)$$

3.2.3 SSIM loss

Besides using l_1 and perceptual losses, to minimize the structural dissimilarities between I_E and I_O , we have included the SSIM loss [70] to our approach. The SSIM is a way to quantify how similar two images are in terms of their structure, luminance, and contrast and can be expressed as:

$$SSIM(c) = \frac{2 \cdot \mu_a \cdot \mu_b + K_1}{\mu_a^2 + \mu_b^2 + K_1} \cdot \frac{2 \cdot \sigma_{ab} + K_2}{\sigma_a^2 + \sigma_b^2 + K_2} \quad (14)$$

where a, b are patches from I_E or I_{SR} , and I_O , respectively, μ , σ , and σ_{ab} denote mean, standard deviation and covariance, given c the center of patches. K_1 and K_2 are fixed parameters. The SSIM loss that we have included in our method can be expressed as follows:

$$l_s = \frac{1}{2n} \sum_{i=1}^n 1 - SSIM(ES(I_{D_i}), I_{O_i}) \quad (15)$$

Finally, our proposed method is trained by minimizing the following losses:

$$l_T = \lambda_1 c l_1 + \lambda_p l_p + \lambda_s l_s \quad (16)$$

where λ_1 , λ_p , and λ_s have been experimentally set to 1, 0.02, and 0.5, respectively.

4 Experiments

In this section, we perform experiments on four popular standard datasets to show the efficacy of our Lit-Net model. Three of them are for underwater image enhancement tasks, namely, EUVP [11], UIEB [7], and SUIM-E [52]. The remaining dataset is for underwater single image super-resolution task, namely, UFO-120 [8]. We evaluate the performance of our Lit-Net model against state-of-the-art approaches and conduct an ablation study to assess the impact of each component of Lit-Net.

Table 1 MSE, PSNR, SSIM, MS-SSIM, LPIPS, UIQM, UISM, and BRISQUE comparison on EUVP dataset with the best-published works for UIE. First, second, and third best performance are represented in red, blue, and green colors, respectively. ↓ indicates lower is better.

Method	MSE↓	PSNR	SSIM	UIQM	LPIPS↓	UISM	MS-SSIM	BRISQUE↓
UGAN [9]	0.355	26.551	0.807	2.896	0.220	6.833	0.936	35.859
UGAN-P [9]	0.347	26.549	0.805	2.931	0.223	6.816	0.935	35.099
FUnIE-GAN[11]	0.386	26.220	0.792	2.971	0.212	6.892	0.924	30.912
FUnIE-GAN-UP	0.600	25.224	0.788	2.935	0.246	6.853	0.925	34.070
Deep SESR [8]	0.325	27.081	0.803	3.099	0.206	7.051	0.940	35.179
DWNNet[6]	0.276	28.654	0.835	3.042	0.173	7.051	0.950	30.856
Ushape [71]	0.370	26.822	0.811	3.052	0.187	6.843	0.949	35.648
Ours	0.225	29.477	0.851	3.027	0.169	7.011	0.954	32.109

4.1 Datasets

4.1.1 EUVP

The EUVP dataset contains 11345 image pairs for underwater enhancement tasks. The testing set consists of 515 paired images. The size of each image is 256×256 .

4.1.2 UIEB

We have used the UIEB dataset for our experiments. It contains 890 image pairs. Following [7], randomly, 800 images choose to train the model, and the remaining 90 images are kept aside for testing the model. We have resized the image into 256×256 for training and testing. Also, we use the 60 challenge images of the UIEB dataset for testing the model without ground truth references.

4.1.3 SUIM-E

The SUIM-E dataset contains a total of 1635 images, out of which 1525 images were used for training and the remaining 110 images were reserved for testing. We make the image size 256×256 for training and testing.

Apart from the datasets mentioned above, we have also used the underwater color cast set (UCCS) [72] and U45 [73] dataset for testing.

4.1.4 UFO-120

We employed the UFO-120 dataset for performing underwater image super-resolution task. It contains 1620 image pairs. We utilized 1500 images for the purpose of training and 120 images for testing. In this dataset, degraded LR images of the dimension 320×240 and the corresponding HR images of the dimension 640×480 are present for $2\times$ super-resolution. To perform $3\times$ and $4\times$ super-resolution, we have down-sample the degraded LR images.

4.2 Experimental Setup

4.2.1 Training Process

The proposed Lit-Net model is implemented based on an open-source deep learning framework called Pytorch. We have performed two independent training for UIE and UISR task. In the training phase, we utilized the Adam optimizer with an initial learning rate of $2e - 4$. All the experiments have been conducted on a Ubuntu 20.04 LTS operating system and one Nvidia A100 GPU. During the training process, a batch size of 5 was employed for the model.

4.2.2 Evaluation Metric

To ensure a fair comparison between the proposed model and existing state-of-the-art approaches, we have assessed the performance of the model using widely used reference and reference-less image quality metrics. These include Mean-squared Error (MSE), Peak Signal-to-Noise Ratio (PSNR), Structural Similarity Index Measure

(SSIM), Multi-scale Structural Similarity Index Measure (MS-SSIM), Learned Perceptual Image Patch Similarity (LPIPS), Underwater Image Quality Measure (UIQM) [74], Underwater Image Sharpness Measure (UISM), and Blind/Reference-less Image Spatial Quality Evaluator (BRISQUE).

4.2.3 State-of-the-Art Methods

- **Underwater Image Enhancement:** In the objective of UIE, the proposed work is compared with several existing state-of-the-art studies, which include: UDCP [18] (*ICCVW* – 13), GBdehaze [21] (*ICASSP* – 16), IBLA [17] (*TIP* – 17), ULAP [22] (*PCM* – 18), CBF [27] (*TIP* – 18), GDGP [16] (*TIP* – 18) UGAN [9] (*ICRA* – 18), WaterNet [7] (*TIP* – 20), UWCNN [35] (*PR* – 20), FUnIE GAN [11] (*RAL* – 20), DeepSESR [8] (*RSS* – 20), UIEC² [75] (*SPIC* – 21), Ucolor [34] (*TIP* – 21), UWCNN-SD [38] (*IJOE* – 21) MILE [76] (*TIP* – 22), PUIE [77] (*ECCV* – 22), SGUIE-Net [52] (*TIP* – 22), UGIF-Net [78] (*TGRS* – 23), DWNet [6] (*TOMM* – 23) and Ushape [71] (*TIP* – 23).
- **Underwater Image Super-resolution:** In the task of UISR, we compare the proposed work against the following best-published methods: SRCNN [79] (*TPAMI* – 16), SRResNet [80] (*CVPR* – 17), SRGAN [80] (*CVPR* – 17), SRDRM [59] (*ICRA* – 20), Deep SESR [8] (*RSS* – 20), and DWNet[6] (*TOMM* – 23).

Our proposed method employs identical training and test sets as other deep learning-based approaches. For a fair comparison, the training and testing image resolution was the same for all the methods as ours. Apart from that, we use the same environment (Python/Matlab) for calculating the measurement metrics.

Table 2 PSNR, SSIM, MS-SSIM, LPIPS, UIQM, UISM, and BRISQUE comparison on UIEB test set with the best-published works for UIE. First, second, and third best performances are represented in red, blue, and green colors, respectively. ↓ indicates lower is better.

Method	PSNR	SSIM	MS-SSIM	LPIPS↓	UIQM	UISM	BRISQUE↓
UDCP [18]	13.026	0.545	0.769	0.283	1.922	7.424	24.133
GBdehaze [21]	15.378	0.671	0.777	0.309	2.520	7.444	23.929
IBLA [17]	19.316	0.690	0.855	0.233	2.108	7.427	23.710
ULAP [22]	19.863	0.724	0.865	0.256	2.328	7.362	25.113
CBF [27]	20.771	0.836	0.890	0.189	3.318	7.380	20.534
UGAN [9]	23.322	0.815	0.932	0.199	3.432	7.241	27.011
UGAN-P [9]	23.550	0.814	0.933	0.192	3.396	7.262	25.382
FUnIE-GAN[11]	21.043	0.785	0.890	0.173	3.250	7.202	24.522
SGUIE-Net [52]	23.496	0.853	0.926	0.136	3.004	7.362	24.607
DWNet [6]	23.165	0.843	0.929	0.162	2.897	7.089	24.863
Ushape [71]	21.084	0.744	0.895	0.220	3.161	7.183	24.128
Ours	23.603	0.863	0.935	0.130	3.145	7.396	23.038

4.3 Comparisons with State-of-the-Arts

Both quantitative and quantitative comparison results of the proposed model with the recent best-published methods are presented in the following subsections:

Table 3 PSNR, SSIM, MS-SSIM, LPIPS, UIQM, UISM, and BRISQUE comparison on SUIM-E test set with the best-published works for UIE. First, second, and third best performances are represented in **red**, **blue**, and **green** colors, respectively. ↓ indicates lower is better

Method	PSNR	SSIM	MS-SSIM	LPIPS↓	UIQM	UISM	BRISQUE↓
UDCP [18]	12.074	0.513	0.742	0.270	1.648	7.537	22.788
GBdehaze [21]	14.339	0.599	0.743	0.355	2.255	7.400	20.175
IBLA [17]	18.024	0.685	0.849	0.209	1.826	7.341	20.957
ULAP [22]	19.148	0.744	0.871	0.231	2.115	7.475	21.250
CBF [27]	20.395	0.834	0.884	0.194	3.003	7.360	21.115
UGAN [9]	24.704	0.826	0.941	0.190	2.894	7.175	20.288
UGAN-P [9]	25.050	0.827	0.943	0.188	2.901	7.184	18.768
FUnIE-GAN[11]	23.590	0.825	0.913	0.189	2.918	7.121	22.560
SGUIE-Net [52]	25.987	0.857	0.945	0.153	2.637	7.090	25.927
DWNet [6]	24.850	0.861	0.941	0.133	2.707	7.381	20.757
Ushape [71]	22.647	0.783	0.917	0.213	2.873	7.061	22.876
Ours	25.117	0.884	0.950	0.118	2.918	7.368	19.602

Table 4 UISM, UIQM, and BRISQUE comparison on UIEB challenge set with the best-published works. First, second, and third best performances are represented in **red**, **blue**, and **green** colors, respectively.

	UDCP [18]	GBdehaze [21]	IBLA [17]	ULAP [22]	CBF [27]	UGAN [9]	FUnIE-GAN [11]	Ucolor [34]	SGUIE-Net [52]	DWNet [6]	Ushape [71]	Ours
UISM	7.358	7.399	7.310	7.239	7.396	7.158	7.140	7.244	7.269	6.677	7.292	7.458
UIQM	1.566	2.280	2.142	1.815	2.810	2.662	2.768	2.483	2.527	2.269	2.783	2.795
BRISQUE↓	29.658	26.264	24.972	30.472	29.213	25.118	24.773	25.093	27.320	31.160	23.616	24.755

4.3.1 Quantitative Evaluation

This sub-section has focused on presenting a quantitative comparison between the proposed method and other existing state-of-the-art approaches with respect to reference and no-reference quality evaluations. The results of these evaluations have been provided in Tables 1, 2, 3, 4, 5 and 7. Table 1, 2, 3, 4, and 5 provide a quantitative comparison of UIE methods. Table 7 presents the evaluation conducted on the task of UISR. Table 1 illustrates that the proposed approach has achieved better results than previous methods for full reference-based quality metrics on the EUVP test set. Besides, Lit-Net also achieves the second and third-best results in terms of non-reference measurement. It is observed that the proposed model has gained improvement on both SSIM and PSNR, 1.92% and 2.87%, respectively. Lit-Net has a low LPIPS score, indicating that the image patches are perceptually more similar to the ground truth. The Lit-Net has surpassed the performance of previous state-of-the-art methods in terms of PSNR, SSIM, and MS-SSIM on the UIEB test dataset,

as demonstrated in Table 2. Additionally, the results also indicate that the proposed model is competitive with the recent schemes in terms of LPIPS and BRISQUE. Table 3 shows that our Lit-Net achieves 2.67% SSIM gains over the previous best methods on the SUIM-E dataset. Our method provides a substantial gain of 0.53% MS-SSIM compared to SGUIE-Net. The corresponding LPIPS score is less, which indicates better perceptual quality. Table 4 demonstrates the UISM, UIQM, and BRISQUE scores of different methods on the UIEB challenge set. The table indicates that the proposed Lit-Net achieves the highest UISM value, second highest BRISQUE value and UIQM value over the state-of-the-art methods. Table 5 demonstrates the quantitative results of U45 and UCCS datasets. The proposed approach attains the top UIQM scores for the UCCS and U45 datasets, respectively. Lit-Net exhibits superior performance on various datasets, implying the model’s robustness. Table 6 shows that our model takes second less number of parameters and GFLOPs. However, this marginal increment also provides a relative performance boost of up to 2.87% and 1.92% regarding PSNR and SSIM over the state-of-the-art on EUVP dataset, which justifies the trade-off between performance and parameters.

Table 5 UIQM comparison on UCCS and U45 datasets with the best-published works. First, second, and third best performances are represented in red, blue, and green colors, respectively.

	GDCP [16]	WaterNet [7]	FUnIE-GAN [11]	UWCNN [35]	UIEC-2 [75]	Ucolor [34]	UWCNN-SD [38]	MLIE [76]	PUIE [77]	UGIF-Net [78]	DWNet [6]	Ours
UCCS	2.716	3.073	3.074	2.981	2.900	2.983	3.130	2.863	2.943	3.112	3.089	3.167
U45	2.370	3.006	2.563	3.110	3.152	3.185	3.134	2.550	2.625	3.264	3.128	3.279

Table 6 Comparison with the model parameters and GFLOPs of the SOTA model with the image size 256×256 . Lower is better.

	WaterNet	UGAN	FUnIE-GAN	Ucolor	SGUIE-Net	DWNet	Ushape	Ours
Parameters (M)	24.8	57.17	7.71	157.4	18.55	0.48	65.6	0.54
FLOPs (G)	193.7	18.3	10.7	443.9	123.5	18.2	66.2	17.8

Table 7 presents the quantitative experiments for single image underwater image super-resolution. It can be inferred from Table 7 that the Lit-Net model has demonstrated superior performance compared to other methods for the task of UISR. We evaluate the performance of our approach against state-of-the-art UISR methods on the UFO-120 test set. Our Lit-Net model obtains the highest PSNR and SSIM scores on a scale of 4, as presented in Table 7, suggesting that our results closely resemble the ground truth regarding visual features. Our method also produces a comparable UIQM result, displaying underwater aspects.

4.3.2 Qualitative Evaluation

In this subsection, we have presented the qualitative performance of the Lit-Net in both the UIE and UISR tasks. Also, we have carried out the qualitative evaluation with the other existing works. The visual comparison of UIE is shown in Fig. 6, 7, 8,

Table 7 PSNR, SSIM, and UIQM comparison on UFO-120 dataset with the best-published works for UISR. First, second, and third best performances are represented in red, blue, and green colors, respectively.

Method	PSNR			SSIM			UIQM		
	2x	3x	4x	2x	3x	4x	2x	3x	4x
SRCNN [79]	24.75 \pm 3.7	22.22 \pm 3.9	19.05 \pm 2.3	.72 \pm .07	.65 \pm .09	.56 \pm .02	2.39 \pm .35	2.24 \pm .17	2.02 \pm .47
SRResNet[80]	25.23 \pm 4.1	23.85 \pm 2.8	19.13 \pm 2.4	.74 \pm .08	.68 \pm .07	.56 \pm .05	2.42 \pm .37	2.18 \pm .26	2.09 \pm .30
SRGAN [80]	26.11 \pm 3.9	23.87 \pm 4.2	21.08 \pm 2.3	.75 \pm .06	.70 \pm .05	.58 \pm .09	2.44 \pm .28	2.39 \pm .25	2.26 \pm .17
SRDRM [59]	24.62 \pm 2.8	-	23.15 \pm 2.9	.72 \pm .17	-	.67 \pm .19	2.59 \pm .64	-	2.56 \pm .63
SRDRM-GAN[59]	24.61 \pm 2.8	-	23.26 \pm 2.8	.72 \pm .17	-	.67 \pm .19	2.59 \pm .64	-	2.57 \pm .63
Deep SESR [8]	25.70 \pm 3.2	26.86 \pm 4.1	24.75 \pm 2.8	.78 \pm .08	.75 \pm .06	.66 \pm .05	3.15 \pm .48	2.87 \pm .39	2.55 \pm .35
DWNet [6]	25.71 \pm 3.0	25.23 \pm 2.7	25.08 \pm 2.9	.80 \pm .08	.79 \pm .10	.74 \pm .14	2.99 \pm .57	2.96 \pm .60	2.97 \pm .59
Ours	25.78 \pm 2.8	25.30 \pm 2.8	25.32 \pm 2.8	.82 \pm .08	.80 \pm .09	.80 \pm .09	3.00 \pm .60	2.99 \pm .57	2.93 \pm .58

and 9. The results displayed in these figures indicate that Lit-Net generates the most visually enhanced images with respect to ground truth. From Fig. 6, one can easily notice that the existing methods IBLA [17] and ULAP [22] fail to recover degraded images. The methods CBF [27] exhibit issues of color deviation in their enhanced images. UGAN [9] and FUnIE-GAN [11] suffer from low contrast. SGUIE-Net [52] provides a better result, but it has a bluishness in the produced image. It can be observed from the third row of Fig. 7 that images produced by the proposed model look more perceptually improved and close to the ground truth. This may be due to the fact that the proposed approach better balances visual quality and color correction. It is also observed from Fig. 8 that the proposed Lit-Net model is capable of handling enhancement effectively, unlike other methods that often result in under and over-saturation, artifacts or fail to correct color deviations. Similar results on the test set of the UIEB challenge are presented in Fig. 9 to show the efficacy of our approach. Our proposed method produces more consistent enhancement over the state-of-art schemes in terms of color correction, contrast enhancement, and detail improvement.

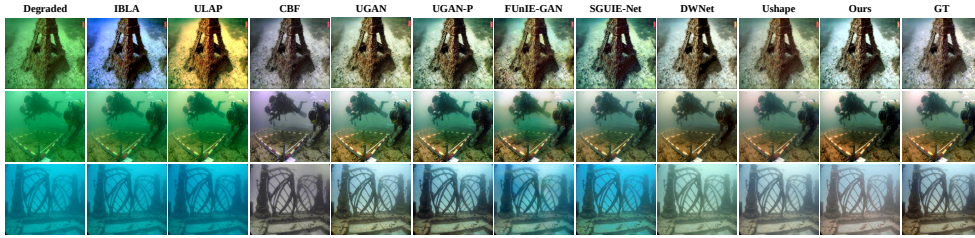


Fig. 6 Visual demonstration against the state-of-the-art UIE models on UIEB dataset.

Fig. 10 and 11 depict the qualitative result for the UISR task. It is observed that SRDRM and SRDRM-GAN [59] can not completely eliminate the color deviations in resulting images. Further, the results achieved using Deep SESR [8] and DWNet [6] still have original noise traces. Fig. 10 and 11 show that Lit-Net produces super-resolution (SR) images with finer texture details and fewer distortions than other recent methods. This demonstrates that Lit-Net is more effective in reducing noise and enhancing image quality. Intuitively, the proposed method has the ability to recreate high-frequency details with sharp edges and fewer unwanted distortions compared to previous methods.

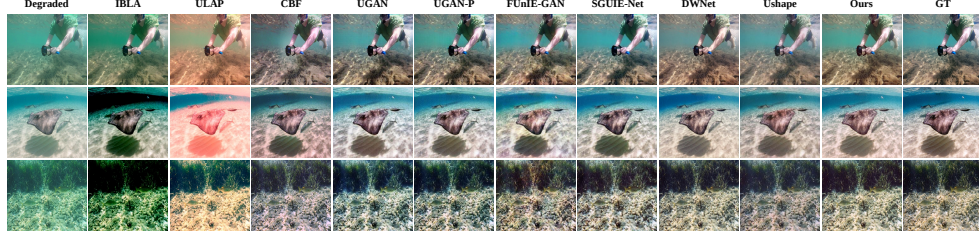


Fig. 7 Visual demonstration against the state-of-the-art UIE models on SUIM-E dataset.

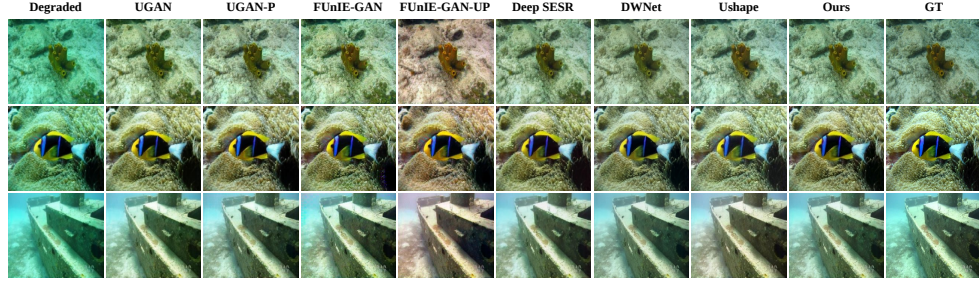


Fig. 8 Visual demonstration against the state-of-the-art UIE models on EUVP dataset.

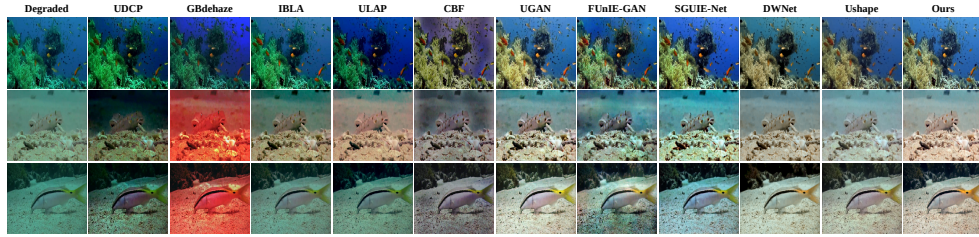


Fig. 9 Visual demonstration against the state-of-the-art UIE models on UIEB challenge test set.

4.4 Ablation Study

In this section, we analyze the contributions of various parameters in the proposed method.

4.4.1 Impact of loss functions

We have performed a series of experiments to demonstrate the influence of various loss functions incorporated in our proposed model. From Table 8, it is evident that l_p loss, when added with cl_1 loss, has improved the UIE performance. The intuitive reason behind such improvement may be the low-level features in the improved images may be benefited from the perceptual loss. Moreover, it is observed from Table that

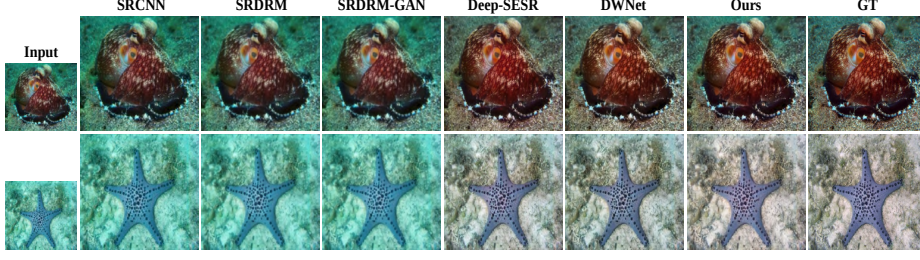


Fig. 10 Visual demonstration against the state-of-the-arts UISR model on UFO-120 dataset for scale 2.

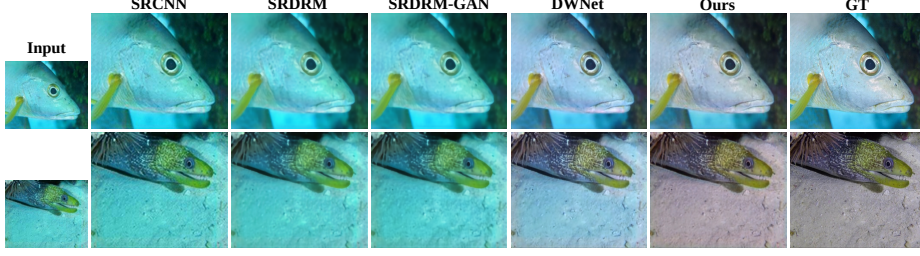


Fig. 11 Visual demonstration against the state-of-the-arts UISR model on UFO-120 dataset for scale 4.

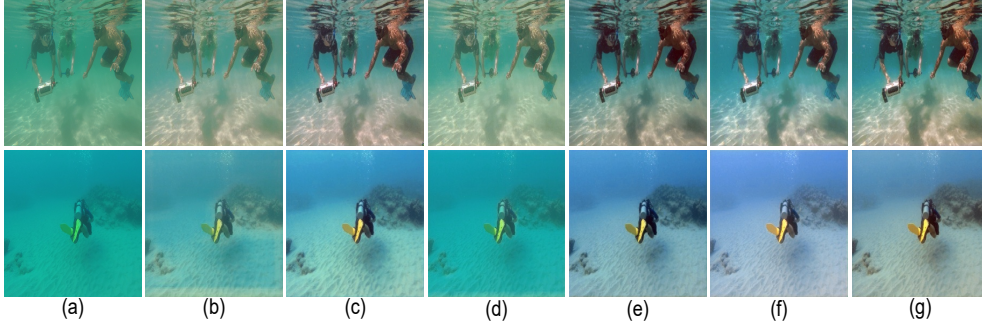


Fig. 12 Visual demonstration of different modules of Lit-Net. (a) Degraded image, (b) MRAN without attention module, (c) MSAN without spatial attention module, (d) Lit-Net without attention module, (e) Lit-Net with fixed size kernel, (f) Lit-Net without channel-wise split, and (g) Full Lit-Net

incorporating the SSIM-based loss function (l_s) has improved the corresponding PSNR and SSIM values noticeably. In the case of underwater SISR, Table 9 shows that the cl_1 loss produces the least amount of performance. Even though the addition of perceptual loss l_p over cl_1 gained performance in a few resolution configurations, there has been a slight improvement, but not in all metrics. Adding l_s loss on top of the earlier losses has improved the performance for all the resolution configurations.

Table 8 Effectiveness of various cost functions on three datasets: EUVP, UIEB, and SUIM-E, for the task of UIE

	EUVP			UIEB			SUIM-E		
	cl_1	$cl_1 + \lambda_p l_p$	$cl_1 + \lambda_p l_p + \lambda_s l_s$	cl_1	$cl_1 + \lambda_p l_p$	$cl_1 + \lambda_p l_p + \lambda_s l_s$	cl_1	$cl_1 + \lambda_p l_p$	$cl_1 + \lambda_p l_p + \lambda_s l_s$
PSNR	29.340	29.095	29.477	22.97	23.593	23.603	24.721	24.899	25.326
SSIM	0.830	0.849	0.851	0.849	0.859	0.863	0.874	0.881	0.884
UIQM	2.980	3.008	3.027	3.118	3.010	3.145	2.819	2.885	2.938

Table 9 Effectiveness of various loss functions on UFO-120 dataset, for the task of UISR

Methods	PSNR			SSIM			UIQM		
	2x	3x	4x	2x	3x	4x	2x	3x	4x
cl_1	23.56	24.97	25.22	.81	.78	.77	2.81	2.90	2.81
$cl_1 + \lambda_p l_p$	24.62	25.02	24.96	.79	.78	.79	2.87	2.96	2.88
$cl_1 + \lambda_p l_p + \lambda_s l_s$	25.78	25.30	25.32	.82	.80	.80	3.00	2.99	2.93

Table 10 Effectiveness of various module on three datasets: UIEB, SUIM-E, and UFO-120(4x) for the task of UIE and UISR

Ablations	GFLOPS Parameter(M)		UIEB			SUIM-E			UFO-120		
			PSNR	SSIM	UIQM	PSNR	SSIM	UIQM	PSNR	SSIM	UIQM
MRAN w/o-Attention	17.852	0.5433	22.958	0.859	3.110	22.230	0.862	2.798	25.137	0.800	2.913
MSAN w/o-Attention	17.863	0.5443	23.255	0.860	3.113	24.499	0.884	2.856	25.156	0.798	2.900
Lit-Net w/o-Attention	17.837	0.5373	20.576	0.832	3.124	21.821	0.854	2.738	25.055	0.796	2.922
Lit-Net w fixed-size kernel	15.912	0.3199	23.568	0.855	3.042	24.871	0.882	2.796	24.814	0.795	2.914
Lit-Net w/o-channel split	14.587	0.4917	22.517	0.854	3.073	24.622	0.872	2.833	24.899	0.803	2.877
Lit-Net w L1 loss	17.871	0.5446	23.530	0.857	3.069	25.003	0.877	2.791	25.066	0.801	2.882
Lit-Net	17.871	0.5446	23.603	0.863	3.145	25.117	0.884	2.918	25.326	0.803	2.938

4.4.2 Effect of Attention Module

In Table 10, we have shown the impact of attention modules in our Lit-Net. We have carried out the experiments on all the datasets. Here, we have presented the result of the UIEB, SUIM-E, and UFO-120 (4x) test sets. From the first, second, and third rows of Table 10, it is observed that the performance of the proposed scheme is relatively low when the attention module is not included in the MRAN block, MSAN block, and the whole Lit-Net. Intuitively, the addition of the CBAM module helps the proposed Lit-Net model to effectively preserve and recover the texture details of the degraded images. As shown in Fig. 12(b), (c), and (d), the enhanced image without the attention module fails to correct the color, local and global contrast.

4.4.3 Effect of different receptive fields and encoder block

To show the effect of receptive fields and encoder block, we have carried out the experiments with the following setup:

1. We have set 3×3 kernel size in the MRAN instead of three different kernels.
2. We have set one 1×1 kernel in the encoder of MSAN instead of four parallel 1×1 .

The fourth row of Table 10 shows a substantial drop in SSIM, PSNR, and UIQM when we have performed the task mentioned above. Notably, Lit-Net with this setting has decreased the 0.15% and 0.98% PSNR value and 3.28% and 4.18% UIQM value on UIEB and SUIM-E datasets, respectively. Fig. 12(e) shows the visual result of the

Lit-Net with these settings. It can be seen that the produced result fails to recover the color.

4.4.4 Effect of weighted color specific L1 loss and color channel split module

The weighted color specific l_1 loss is designed to correct the color, which is affected by the wavelength of the underwater medium. The sixth row of Table 10 shows the result of our method with l_1 loss along with other losses. It is observed that the proposed method with l_1 loss has decreased the PSNR, SSIM, and UIQM values as compared to cl_1 loss.

Similar to color-specific loss, Lit-Net processes the R, G, and B channels with different kernel sizes to capture the global context from the blue channel and the local context from the red channel. When the proposed method processes the entire RGB image instead of employing R, G, and B channel-wise processing, it can be observed from the 5th row of Table 10, Lit-Net provides a decrease of 1.086 dB, 0.495 dB, and 0.427 dB PSNR. Compared with Lit-Net w/o-channel split, the full model improves the UIQM score with 2.29%, 2.91%, and 2.08% on UIEB, SUIM-E, and UFO-120 (4X) test set, respectively. Fig. 12(f) shows the visual quality of Lit-Net w/o-channel split, it is less sharp and fails to recover the details. Fig. 12(g) shows that the full Lit-Net provides better color correction, detail recovery, and perceptual enhancement.

4.5 Impact on High level Vision Applications

We have demonstrated the resilience of the improved images generated by the Lit-Net against state-of-the-art UIR strategies on several underwater high-level vision applications. We have taken into account tasks like underwater object detection and single-image semantic segmentation for this.

4.5.1 Underwater Semantic Segmentation

Semantic segmentation is a process of labelling or assigning a category to each pixel in an image. This technique is utilized to identify a group of pixels that collectively belong to separate categories for detailed scene understanding. We have used the SUIM dataset [81] for underwater semantic segmentation. First, we enhance the images in the SUIM dataset using our proposed Lit-Net. Second, we utilized the SUIM-Net [81] method for the semantic segmentation task to show the performance gain by using the enhanced images. Fig. 13 shows that generated segmentation maps are more refined than existing ones.

4.5.2 Underwater Object Detection

To validate the impact of UIE on object detection tasks, we utilize the improved outcomes in a detection algorithm. For this task, we have used the YOLOv5 [82] and Aquarium dataset [83]. We have reported the quantitative results in Table 11. The results indicate that the proposed method exhibits better detection accuracy than the other competitive methods. Fig. 14 displays the visualization of detection results

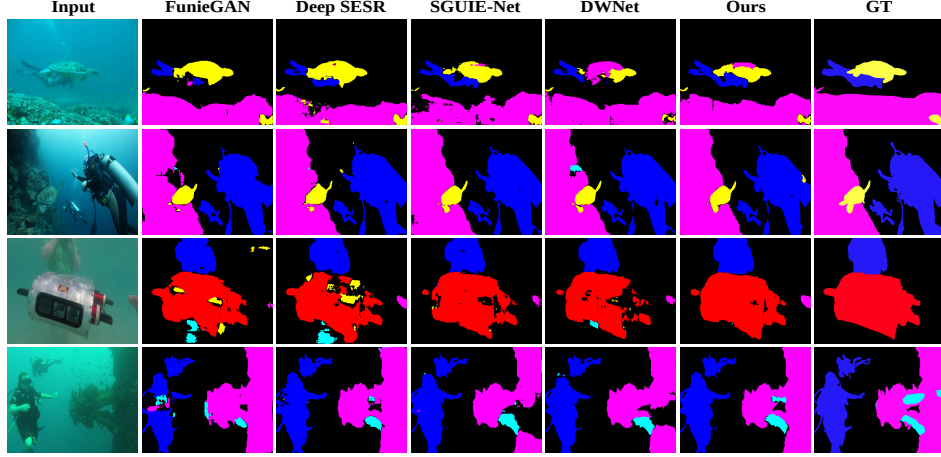


Fig. 13 Visual comparison of the semantic segmentation maps derived from the improved underwater images from four existing UIE works.

Table 11 Mean average precision (mAP) comparison on detection task

	Fish	Jellyfish	Penguin	Puffin	Shark	Starfish	Stingray	All
Degraded	0.815	0.929	0.749	0.602	0.749	0.838	0.781	0.780
FUNIE-GAN	0.744	0.923	0.654	0.445	0.664	0.716	0.755	0.700
Deep SESR	0.706	0.943	0.643	0.41	0.638	0.703	0.757	0.686
DWNNet	0.839	0.948	0.752	0.551	0.757	0.819	0.806	0.782
Lit-Net	0.821	0.940	0.753	0.615	0.785	0.841	0.814	0.796

obtained on the Aquarium dataset. It is shown in Fig. 14 that in spite of visual enhancement, FUNIEGAN [11], Deep SESR [8], and DWNNet [6] methods showed inferior results for the detection performance in comparison with proposed Lit-Net model.

4.6 Failure Case

We examine a few failure cases of Lit-Net, as depicted in Figure 15. Our approach needs to perform well in a few cases where the rate degradation is highly intense, such as extremely low contrast, irregular coloring, etc. For example, in the first image, the GT image contains color for the object and sea grass, and it is almost difficult to observe its color in the predicted image because it is tough to identify the colors from the original degraded image. As illustrated in the second image, the contrast of the lower left region is extremely diverse from the contrast of the lower region. Since our model lacks explicit provisions for extremely low-light image enhancement, a few resultant images may exhibit a tendency towards suboptimal enhancement. In the future, we can introduce extremely low-light correction modules to precisely enhance images with uneven illumination.

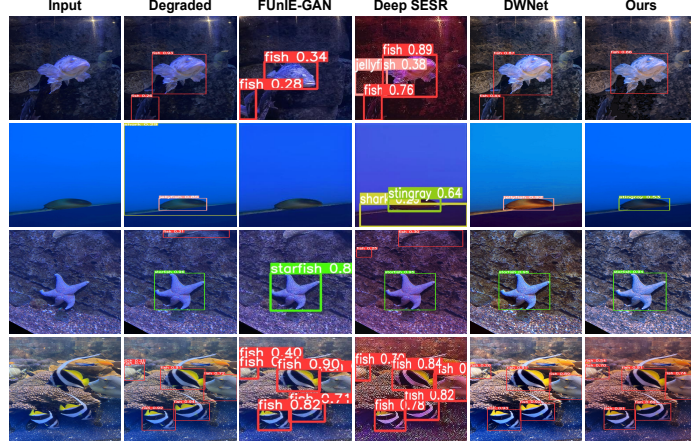


Fig. 14 Visual demonstration of object detection by utilizing the improved images from three existing UIE works.

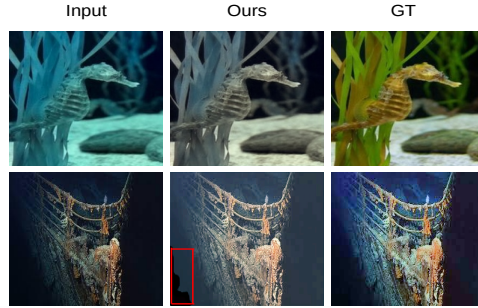


Fig. 15 Visual demonstration of object detection by utilizing the improved images from three existing UIE works.

5 Conclusion

In this paper, a novel light-weight image enhancement and super resolution model, called Lit-Net, is proposed specifically for underwater images. In this model, there are two main modules, namely Multi-resolution Attention Network (MRAN) and Multi-scale Attention Network (MSAN). Different receptive fields (different convolution kernels) have been used to achieve the multi-resolution image analysis while retaining the original input resolution. In the MSAN module, we have used spatial attention based skip connections between respective encoder-decoder layers to get both semantically and spatially rich feature representations. We also demonstrated that employing this type of encoder design aids in learning diverse features and reduces the complexity of the model. Furthermore, we used the weighted color channel specific l_1 loss which enhances the performance of Lit-Net. Experiments on both UIE and UISR show

that the proposed Lit-Net outperforms the state-of-the-art methods. We also provided an ablation studies to justify the contribution of different modules. It is also experimentally demonstrated that the images, enhanced with the proposed model, achieve significant improvements in the performance of various advanced visual tasks, such as underwater object detection and semantic segmentation.

References

- [1] Rokh, B., Azarpeyvand, A., Khanteymooori, A.: A comprehensive survey on model quantization for deep neural networks in image classification. *ACM Transactions on Intelligent Systems and Technology* **14**(6), 1–50 (2023)
- [2] Xu, S., Zhang, M., Song, W., Mei, H., He, Q., Liotta, A.: A systematic review and analysis of deep learning-based underwater object detection. *Neurocomputing* **527**, 204–232 (2023)
- [3] Yi, D., Ahmedov, H.B., Jiang, S., Li, Y., Flinn, S.J., Fernandes, P.G.: Coordinate-aware mask r-cnn with group normalization: A underwater marine animal instance segmentation framework. *Neurocomputing* **583**, 127488 (2024)
- [4] Chiang, J.Y., Chen, Y.-C.: Underwater image enhancement by wavelength compensation and dehazing. *IEEE trans. on image process.* **21**(4), 1756–1769 (2011)
- [5] Raveendran, S., Patil, M.D., Birajdar, G.K.: Underwater image enhancement: a comprehensive review, recent trends, challenges and applications. *Artificial Intelligence Review* **54**, 5413–5467 (2021)
- [6] Sharma, P., Bisht, I., Sur, A.: Wavelength-based attributed deep neural network for underwater image restoration. *ACM Transactions on Multimedia Computing, Communications and Applications* **19**(1), 1–23 (2023)
- [7] Li, C., Guo, C., Ren, W., Cong, R., Hou, J., Kwong, S., Tao, D.: An underwater image enhancement benchmark dataset and beyond. *IEEE Transactions on Image Processing* **29**, 4376–4389 (2019)
- [8] Islam, M.J., Luo, P., Sattar, J.: Simultaneous enhancement and super-resolution of underwater imagery for improved visual perception. *arXiv preprint arXiv:2002.01155* (2020)
- [9] Fabbri, C., Islam, M.J., Sattar, J.: Enhancing underwater imagery using generative adversarial networks. In: 2018 IEEE International Conference on Robotics and Automation (ICRA), pp. 7159–7165 (2018). IEEE
- [10] Chen, Z., Qiu, G., Li, P., Zhu, L., Yang, X., Sheng, B.: Mngnas: distilling adaptive combination of multiple searched networks for one-shot neural architecture search. *IEEE Transactions on Pattern Analysis and Machine Intelligence* (2023)

- [11] Islam, M.J., Xia, Y., Sattar, J.: Fast underwater image enhancement for improved visual perception. *IEEE Robotics and Automation Letters* **5**(2), 3227–3234 (2020)
- [12] Szegedy, C., Liu, W., Jia, Y., Sermanet, P., Reed, S., Anguelov, D., Erhan, D., Vanhoucke, V., Rabinovich, A.: Going deeper with convolutions. In: *Proceedings of the IEEE Conference on Computer Vision and Pattern Recognition*, pp. 1–9 (2015)
- [13] Drews, P.L., Nascimento, E.R., Botelho, S.S., Campos, M.F.M.: Underwater depth estimation and image restoration based on single images. *IEEE computer graphics and applications* **36**(2), 24–35 (2016)
- [14] Galdran, A., Pardo, D., Picón, A., Alvarez-Gila, A.: Automatic red-channel underwater image restoration. *Journal of Visual Communication and Image Representation* **26**, 132–145 (2015)
- [15] Li, C.-Y., Guo, J.-C., Cong, R.-M., Pang, Y.-W., Wang, B.: Underwater image enhancement by dehazing with minimum information loss and histogram distribution prior. *IEEE Transactions on Image Processing* **25**(12), 5664–5677 (2016)
- [16] Peng, Y.-T., Cao, K., Cosman, P.C.: Generalization of the dark channel prior for single image restoration. *IEEE Transactions on Image Processing* **27**(6), 2856–2868 (2018)
- [17] Peng, Y.-T., Cosman, P.C.: Underwater image restoration based on image blurriness and light absorption. *IEEE transactions on image processing* **26**(4), 1579–1594 (2017)
- [18] Drews, P., Nascimento, E., Moraes, F., Botelho, S., Campos, M.: Transmission estimation in underwater single images. In: *Proceedings of the IEEE International Conference on Computer Vision Workshops*, pp. 825–830 (2013)
- [19] He, K., Sun, J., Tang, X.: Single image haze removal using dark channel prior. *IEEE transactions on pattern analysis and machine intelligence* **33**(12), 2341–2353 (2010)
- [20] Wen, H., Tian, Y., Huang, T., Gao, W.: Single underwater image enhancement with a new optical model. In: *2013 IEEE International Symposium on Circuits and Systems (ISCAS)*, pp. 753–756 (2013). IEEE
- [21] Li, C., Quo, J., Pang, Y., Chen, S., Wang, J.: Single underwater image restoration by blue-green channels dehazing and red channel correction. In: *2016 IEEE International Conference on Acoustics, Speech and Signal Processing (ICASSP)*, pp. 1731–1735 (2016). IEEE

- [22] Song, W., Wang, Y., Huang, D., Tjondronegoro, D.: A rapid scene depth estimation model based on underwater light attenuation prior for underwater image restoration. In: *Advances in Multimedia Information Processing–PCM 2018: 19th Pacific-Rim Conference on Multimedia*, Hefei, China, September 21-22, 2018, *Proceedings, Part I* 19, pp. 678–688 (2018). Springer
- [23] Ouyang, T., Zhang, Y., Zhao, H., Cui, Z., Yang, Y., Xu, Y.: A multi-color and multistage collaborative network guided by refined transmission prior for underwater image enhancement. *The Visual Computer*, 1–19 (2024)
- [24] Akkaynak, D., Treibitz, T.: Sea-thru: A method for removing water from underwater images. In: *Proceedings of the IEEE/CVF Conference on Computer Vision and Pattern Recognition*, pp. 1682–1691 (2019)
- [25] Akkaynak, D., Treibitz, T.: A revised underwater image formation model. In: *Proceedings of the IEEE Conference on Computer Vision and Pattern Recognition*, pp. 6723–6732 (2018)
- [26] Akkaynak, D., Treibitz, T., Shlesinger, T., Loya, Y., Tamir, R., Iluz, D.: What is the space of attenuation coefficients in underwater computer vision? In: *Proceedings of the IEEE Conference on Computer Vision and Pattern Recognition*, pp. 4931–4940 (2017)
- [27] Ancuti, C.O., Ancuti, C., De Vleeschouwer, C., Bekaert, P.: Color balance and fusion for underwater image enhancement. *IEEE Transactions on image processing* **27**(1), 379–393 (2017)
- [28] Ancuti, C.O., Ancuti, C., Haber, T., Bekaert, P.: Fusion-based restoration of the underwater images. In: *2011 18th IEEE International Conference on Image Processing*, pp. 1557–1560 (2011). IEEE
- [29] Aguirre-Castro, O.A., García-Guerrero, E.E., López-Bonilla, O.R., Tlelo-Cuautle, E., López-Mancilla, D., Cárdenas-Valdez, J.R., Olguín-Tiznado, J.E., Inzunza-González, E.: Evaluation of underwater image enhancement algorithms based on retinex and its implementation on embedded systems. *Neurocomputing* **494**, 148–159 (2022)
- [30] Fu, X., Zhuang, P., Huang, Y., Liao, Y., Zhang, X.-P., Ding, X.: A retinex-based enhancing approach for single underwater image. In: *2014 IEEE International Conference on Image Processing (ICIP)*, pp. 4572–4576 (2014). IEEE
- [31] Ghani, A.S.A., Isa, N.A.M.: Underwater image quality enhancement through integrated color model with rayleigh distribution. *Applied soft computing* **27**, 219–230 (2015)
- [32] Xue, Q., Hu, H., Bai, Y., Cheng, R., Wang, P., Song, N.: Underwater image enhancement algorithm based on color correction and contrast enhancement. *The*

- [33] Qiao, N., Di, L.: Underwater image enhancement combining low-dimensional and global features. *The Visual Computer* **39**(7), 3029–3039 (2023)
- [34] Li, C., Anwar, S., Hou, J., Cong, R., Guo, C., Ren, W.: Underwater image enhancement via medium transmission-guided multi-color space embedding. *IEEE Transactions on Image Processing* **30**, 4985–5000 (2021)
- [35] Li, C., Anwar, S., Porikli, F.: Underwater scene prior inspired deep underwater image and video enhancement. *Pattern Recognition* **98**, 107038 (2020)
- [36] Li, J., Skinner, K.A., Eustice, R.M., Johnson-Roberson, M.: Watergan: Unsupervised generative network to enable real-time color correction of monocular underwater images. *IEEE Robotics and Automation letters* **3**(1), 387–394 (2017)
- [37] Uplavikar, P.M., Wu, Z., Wang, Z.: All-in-one underwater image enhancement using domain-adversarial learning. In: *CVPR Workshops*, pp. 1–8 (2019)
- [38] Wu, S., Luo, T., Jiang, G., Yu, M., Xu, H., Zhu, Z., Song, Y.: A two-stage underwater enhancement network based on structure decomposition and characteristics of underwater imaging. *IEEE Journal of Oceanic Engineering* **46**(4), 1213–1227 (2021)
- [39] Tolia, H.F., Ren, J., Elyan, E.: Dicam: Deep inception and channel-wise attention modules for underwater image enhancement. *Neurocomputing* **584**, 127585 (2024)
- [40] Tao, Y., Tang, J., Zhao, X., Zhou, C., Wang, C., Zhao, Z.: Multi-scale network with attention mechanism for underwater image enhancement. *Neurocomputing*, 127926 (2024)
- [41] Lai, Y., Xu, H., Lin, C., Luo, T., Wang, L.: A two-stage and two-branch generative adversarial network-based underwater image enhancement. *The Visual Computer* **39**(9), 4133–4147 (2023)
- [42] Guo, Y., Li, H., Zhuang, P.: Underwater image enhancement using a multi-scale dense generative adversarial network. *IEEE Journal of Oceanic Engineering* **45**(3), 862–870 (2019)
- [43] Goodfellow, I., Pouget-Abadie, J., Mirza, M., Xu, B., Warde-Farley, D., Ozair, S., Courville, A., Bengio, Y.: Generative adversarial nets. *Advances in neural information processing systems* **27** (2014)
- [44] Liu, P., Wang, G., Qi, H., Zhang, C., Zheng, H., Yu, Z.: Underwater image enhancement with a deep residual framework. *IEEE Access* **7**, 94614–94629 (2019)

- [45] Engin, D., Genç, A., Kemal Ekenel, H.: Cycle-dehaze: Enhanced cyclegan for single image dehazing. In: Proceedings of the IEEE Conference on Computer Vision and Pattern Recognition Workshops, pp. 825–833 (2018)
- [46] Kim, J., Lee, J.K., Lee, K.M.: Accurate image super-resolution using very deep convolutional networks. In: Proceedings of the IEEE Conference on Computer Vision and Pattern Recognition, pp. 1646–1654 (2016)
- [47] Wang, J., Li, P., Deng, J., Du, Y., Zhuang, J., Liang, P., Liu, P.: Ca-gan: Class-condition attention gan for underwater image enhancement. *IEEE Access* **8**, 130719–130728 (2020)
- [48] Vaswani, A., Shazeer, N., Parmar, N., Uszkoreit, J., Jones, L., Gomez, A.N., Kaiser, Ł., Polosukhin, I.: Attention is all you need. *Advances in neural information processing systems* **30** (2017)
- [49] Lin, X., Sun, S., Huang, W., Sheng, B., Li, P., Feng, D.D.: Eapt: efficient attention pyramid transformer for image processing. *IEEE Transactions on Multimedia* **25**, 50–61 (2021)
- [50] Han, R., Guan, Y., Yu, Z., Liu, P., Zheng, H.: Underwater image enhancement based on a spiral generative adversarial framework. *IEEE Access* **8**, 218838–218852 (2020)
- [51] Huo, F., Li, B., Zhu, X.: Efficient wavelet boost learning-based multi-stage progressive refinement network for underwater image enhancement. In: Proceedings of the IEEE/CVF International Conference on Computer Vision, pp. 1944–1952 (2021)
- [52] Qi, Q., Li, K., Zheng, H., Gao, X., Hou, G., Sun, K.: Sguie-net: Semantic attention guided underwater image enhancement with multi-scale perception. *IEEE Transactions on Image Processing* **31**, 6816–6830 (2022)
- [53] Jin, Z., Iqbal, M.Z., Bobkov, D., Zou, W., Li, X., Steinbach, E.: A flexible deep cnn framework for image restoration. *IEEE Transactions on Multimedia* **22**(4), 1055–1068 (2019)
- [54] Tian, C., Xu, Y., Zuo, W., Zhang, B., Fei, L., Lin, C.-W.: Coarse-to-fine cnn for image super-resolution. *IEEE Transactions on Multimedia* **23**, 1489–1502 (2020)
- [55] Yang, W., Zhang, X., Tian, Y., Wang, W., Xue, J.-H., Liao, Q.: Deep learning for single image super-resolution: A brief review. *IEEE Transactions on Multimedia* **21**(12), 3106–3121 (2019)
- [56] Zhang, Y., Tian, Y., Kong, Y., Zhong, B., Fu, Y.: Residual dense network for image super-resolution. In: Proceedings of the IEEE Conference on Computer Vision and Pattern Recognition, pp. 2472–2481 (2018)

- [57] Chen, Y., Niu, K., Zeng, Z., Pan, Y.: A wavelet based deep learning method for underwater image super resolution reconstruction. *IEEE Access* **8**, 117759–117769 (2020)
- [58] Lu, H., Li, Y., Nakashima, S., Kim, H., Serikawa, S.: Underwater image super-resolution by descattering and fusion. *IEEE Access* **5**, 670–679 (2017)
- [59] Islam, M.J., Enan, S.S., Luo, P., Sattar, J.: Underwater image super-resolution using deep residual multipliers. In: 2020 IEEE International Conference on Robotics and Automation (ICRA), pp. 900–906 (2020). IEEE
- [60] Zhang, Y., Yang, S., Sun, Y., Liu, S., Li, X.: Attention-guided multi-path cross-cnn for underwater image super-resolution. *Signal, Image and Video Processing* **16**(1), 155–163 (2022)
- [61] Zhang, Y., Jiang, Q., Liu, P., Gao, S., Pan, X., Zhang, C.: Underwater image enhancement using deep transfer learning based on a color restoration model. *IEEE Journal of Oceanic Engineering* **48**(2), 489–514 (2023)
- [62] Dudhane, A., Patil, P.W., Murala, S.: An end-to-end network for image de-hazing and beyond. *IEEE Transactions on Emerging Topics in Computational Intelligence* **6**(1), 159–170 (2020)
- [63] Dharejo, F.A., Deeba, F., Zhou, Y., Das, B., Jatoi, M.A., Zawish, M., Du, Y., Wang, X.: Twist-gan: Towards wavelet transform and transferred gan for spatio-temporal single image super resolution. *ACM Transactions on Intelligent Systems and Technology (TIST)* **12**(6), 1–20 (2021)
- [64] Jiang, N., Sheng, B., Li, P., Lee, T.-Y.: Photohelper: portrait photographing guidance via deep feature retrieval and fusion. *IEEE Transactions on Multimedia* **25**, 2226–2238 (2022)
- [65] Woo, S., Park, J., Lee, J.-Y., Kweon, I.S.: Cbam: Convolutional block attention module. In: Proceedings of the European Conference on Computer Vision (ECCV), pp. 3–19 (2018)
- [66] Ioffe, S., Szegedy, C.: Batch normalization: Accelerating deep network training by reducing internal covariate shift. In: International Conference on Machine Learning, pp. 448–456 (2015). pmlr
- [67] Shi, W., Caballero, J., Huszár, F., Totz, J., Aitken, A.P., Bishop, R., Rueckert, D., Wang, Z.: Real-time single image and video super-resolution using an efficient sub-pixel convolutional neural network. In: Proceedings of the IEEE Conference on Computer Vision and Pattern Recognition, pp. 1874–1883 (2016)
- [68] Johnson, J., Alahi, A., Fei-Fei, L.: Perceptual losses for real-time style transfer

- and super-resolution. In: Computer Vision–ECCV 2016: 14th European Conference, Amsterdam, The Netherlands, October 11–14, 2016, Proceedings, Part II 14, pp. 694–711 (2016). Springer
- [69] Simonyan, K., Zisserman, A.: Very deep convolutional networks for large-scale image recognition. arXiv preprint arXiv:1409.1556 (2014)
 - [70] Wang, Z., Bovik, A.C., Sheikh, H.R., Simoncelli, E.P.: Image quality assessment: from error visibility to structural similarity. IEEE transactions on image processing **13**(4), 600–612 (2004)
 - [71] Peng, L., Zhu, C., Bian, L.: U-shape transformer for underwater image enhancement. IEEE Transactions on Image Processing (2023)
 - [72] Liu, R., Fan, X., Zhu, M., Hou, M., Luo, Z.: Real-world underwater enhancement: Challenges, benchmarks, and solutions under natural light. IEEE transactions on circuits and systems for video technology **30**(12), 4861–4875 (2020)
 - [73] Li, H., Li, J., Wang, W.: A fusion adversarial underwater image enhancement network with a public test dataset. arXiv preprint arXiv:1906.06819 (2019)
 - [74] Panetta, K., Gao, C., Agaian, S.: Human-visual-system-inspired underwater image quality measures. IEEE Journal of Oceanic Engineering **41**(3), 541–551 (2015)
 - [75] Wang, Y., Guo, J., Gao, H., Yue, H.: Uiec²-net: Cnn-based underwater image enhancement using two color space. Signal Processing: Image Communication **96**, 116250 (2021)
 - [76] Zhang, W., Zhuang, P., Sun, H.-H., Li, G., Kwong, S., Li, C.: Underwater image enhancement via minimal color loss and locally adaptive contrast enhancement. IEEE Transactions on Image Processing **31**, 3997–4010 (2022)
 - [77] Fu, Z., Wang, W., Huang, Y., Ding, X., Ma, K.-K.: Uncertainty inspired underwater image enhancement. In: European Conference on Computer Vision, pp. 465–482 (2022). Springer
 - [78] Zhou, J., Li, B., Zhang, D., Yuan, J., Zhang, W., Cai, Z., Shi, J.: Ugif-net: An efficient fully guided information flow network for underwater image enhancement. IEEE Transactions on Geoscience and Remote Sensing (2023)
 - [79] Dong, C., Loy, C.C., He, K., Tang, X.: Image super-resolution using deep convolutional networks. IEEE transactions on pattern analysis and machine intelligence **38**(2), 295–307 (2015)
 - [80] Ledig, C., Theis, L., Huszár, F., Caballero, J., Cunningham, A., Acosta, A., Aitken, A., Tejani, A., Totz, J., Wang, Z., *et al.*: Photo-realistic single image

- super-resolution using a generative adversarial network. In: Proceedings of the IEEE Conference on Computer Vision and Pattern Recognition, pp. 4681–4690 (2017)
- [81] Islam, M.J., Edge, C., Xiao, Y., Luo, P., Mehtaz, M., Morse, C., Enan, S.S., Sattar, J.: Semantic Segmentation of Underwater Imagery: Dataset and Benchmark. In: IEEE/RSJ International Conference on Intelligent Robots and Systems (IROS) (2020). IEEE/RSJ
- [82] Jocher, G., Chaurasia, A., Stoken, A., et al.: YOLOv5. <https://github.com/ultralytics/yolov5> (2020)
- [83] Roboflow: Aquarium Dataset. <https://public.roboflow.com/object-detection/aquarium> (2020)